Available online at www.sciencedirect.com
ScienceDirect
Journal of Power Sources 161 (2006) 957–964
JOURNAL OF POWER SOURCES
www.elsevier.com/locate/jpowsour

Thermodynamics of SOFC efficiency and fuel utilization as functions of fuel mixtures and operating conditions

Huayang Zhu*, Robert J. Kee

Engineering Division, Colorado School of Mines, Golden, CO 80401, USA

Received 31 March 2006; received in revised form 6 May 2006; accepted 8 May 2006
Available online 23 June 2006

Abstract

This paper develops a new thermodynamic model that predicts maximum fuel-cell efficiency and fuel utilization as a function of fuel composition and operating conditions. Interestingly, it is shown that maximum possible efficiency is independent of membrane-electrode assembly characteristics and internal polarization losses. However, because the power density depends on internal polarization losses, the cell size needed to achieve maximum efficiency depends greatly on cell architecture. A very detailed fuel-cell model is used to validate the thermodynamic model and to provide further insight on practical considerations such as power density. The model is illustrated using solid-oxide fuel cell examples.
© 2006 Elsevier B.V. All rights reserved.

Keywords: SOFC; Fuel-cell efficiency; Fuel utilization; Thermodynamic modeling

1. Introduction

It is well known that fuel cells promise the potential for very high efficiency in the conversion of hydrogen or hydrocarbon to electricity. However, precise definitions of efficiency can vary widely [1–3]. In a narrow sense, an efficiency can be defined for the fuel cell alone. In a broad sense, efficiency must consider the entire system, including all balance-of-plant components. Because full-system designs can vary greatly, it is difficult, if not impossible, to generalize the analysis of efficiency. The objective of the present paper is to develop purely general thermodynamic models that characterize efficiency of the fuel cell alone.

An interesting and remarkable result of the thermodynamic analysis is that maximum fuel-cell efficiency is independent of internal polarization losses. However, power densities depend strongly on internal losses. To achieve maximum efficiency, the cell size depends on power density and hence on the structure and performance-characteristics of the cell. To assist interpretation of the thermodynamic models, this paper also uses a very detailed model of solid-oxide fuel cells (SOFC). The detailed model considers specific membrane-electrode assembly (MEA) structure, reactive porous-media transport, electrochemical charge transfer, and elementary heterogeneous reforming chemistry [4].

The thermodynamic analysis developed in this paper is both general and restrictive. It is general in the sense that it accommodates different fuels, flow rates, temperatures, and pressures. Because maximum efficiency and fuel utilization are thermodynamic functions, they do not depend on particular MEA structure or cell design. However, the analysis is also restrictive. Isothermal operation is assumed and all gases entering the fuel cell are assumed to be at the cell operating temperature. Thus, the cost of heating inlet streams (especially the air) must be accommodated in balance-of-plant models that consider heat-exchanger performance. The models presume that charge transfer proceeds via H_2. When the parent fuel is a hydrocarbon internal reforming is assumed to proceed to equilibrium.

Although the thermodynamic model has restrictions and assumptions, the results are highly informative and practically useful. Overall thermal management of an entire system is critically important. However, the thermodynamic model developed here can be integrated into a larger system model. The assumption of hydrogen charge transfer is a very reasonable one, and does not affect the overall greatly.

The thermal efficiency of any energy-conversion device can be defined as the ratio of useful work done W_{out} and the potential

* Corresponding author. Tel.: +1 303 273 3890; fax: +1 303 273 3602.
E-mail address: hzhu@mines.edu (H. Zhu).

0378-7753/$ – see front matter © 2006 Elsevier B.V. All rights reserved.
doi:10.1016/j.jpowsour.2006.05.006

of the inlet stream to do work Q_{in}; that is $\varepsilon = W_{out}/Q_{in}$. For a fuel-cell system, the useful work is electric power W_e, which is the product of the electric current density i and operating voltage E_{cell}, integrated over the active MEA area, $W_e = \int i E_{cell}\, dA$. The potential to do work can be represented in terms of the heat-release associated with full oxidation of the inlet fuel stream, $Q_{in} = \dot{m}_{f,in}\, \Delta h_{f,in}$. Here the inlet fuel mass flow rate is $\dot{m}_{f,in}$ and $\Delta h_{f,in}$ is the specific enthalpy associated with completely oxidizing the fuel stream. With these definitions in mind, the net fuel-cell efficiency can be defined as,

$$\varepsilon = \frac{W_e}{Q_{in}} = \frac{\int i E_{cell}\, dA}{\dot{m}_{f,in}\, \Delta h_{f,in}}. \quad (1)$$

The efficiency of a fuel-cell system can be written as the product of three contributing efficiencies [5]: the reversible efficiency ε_R, the voltage or part-load efficiency ε_V, and the fuel utilization ε_U,

$$\varepsilon = \varepsilon_R \varepsilon_V \varepsilon_U. \quad (2)$$

The ideal efficiency, or the reversible efficiency, ε_R is written as

$$\varepsilon_R = \frac{\Delta G}{\Delta H} = 1 - T\frac{\Delta S}{\Delta H}, \quad (3)$$

where ΔG, ΔH, and ΔS are the changes in molar free energy, enthalpy, and entropy, respectively, associated with full oxidation of the fuel.

Any overpotential losses within the fuel cell reduce the cell potential when it is operated under load. Thus, the net efficiency depends on the operating cell potential E_{cell}. A part-load efficiency or the voltage efficiency is defined as

$$\varepsilon_V = \frac{E_{cell}}{E_{rev}}, \quad (4)$$

where E_{rev} is the reversible (Nernst) potential. Thorstensen [5] proposed that overall cell efficiency should be the product of the reversible efficiency and the part-load efficiency as,

$$\varepsilon = \varepsilon_R \varepsilon_V. \quad (5)$$

Ferguson and Ugursal improved this approach by incorporating activation-polarization losses using a two-linear-segment polarization curve [6].

Fuel utilization also strongly affects the efficiency. Consider an SOFC system, where fuel is electrochemically oxidized along the length of an anode channel. As the fuel is consumed, the anode fuel stream is also diluted by reaction products (i.e., H_2O and CO_2). As the fuel concentration decreases along the length of the anode channel, the reversible potential E_{rev} decreases.

As long as the reversible potential exceeds the cell operating potential (i.e., $E_{rev} > E_{cell}$) the cell can produce electric current. However, once E_{rev} equals E_{cell}, no more fuel can be consumed and no more current can be produced. Any unused fuels in the exhaust reduce the fuel-cell efficiency. Fuel utilization ε_U can be written as

$$\varepsilon_U = 1 - \frac{\dot{m}_{f,out}\, \Delta h_{f,out}}{\dot{m}_{f,in}\, \Delta h_{f,in}}, \quad (6)$$

where the "in" and "out" refer to the inlet and outlet of the fuel cell. The Δh refers to the specific enthalpy associated with complete oxidation of any available fuels. This definition accounts for the energy content of any remaining fuels (or fuel byproducts) that leave in the fuel-cell exhaust. For example, even though essentially all the parent fuel (e.g., a hydrocarbon) is consumed in the sense it is no longer present in the anode exhaust, there may still be considerable energy available in the form of other hydrocarbons or CO and H_2.

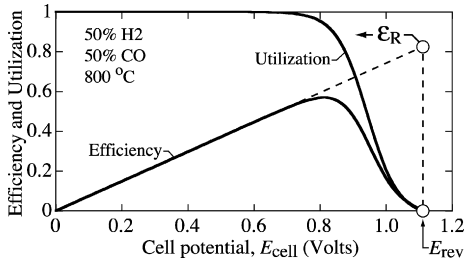

Fig. 1. Fuel-cell efficiency and fuel utilization as functions of operating cell voltage in an SOFC. The fuel stream is based on the equilibrium state of 50% H_2 and 50% CO at the temperature of 800 °C and atmospheric pressure.

Fig. 1 illustrates the typical behavior of the fuel-cell efficiency and fuel utilization as functions of operating cell voltage for a given fuel stream and operating conditions. Operating at low cell potential, the fuel can be fully utilized and the fuel-cell efficiency is a linear function of cell potential E_{cell}. The slope of this function depends on fuel composition as well as operating temperature and pressure.

The reversible efficiency ε_R, which can be determined thermodynamically (Eq. (3)), is shown as a circle in Fig. 1. The reversible efficiency, which would be achieved by operating the cell at its reversible potential, cannot be achieved in practice because of low fuel utilization at high operating potential. The efficiency reaches a maximum at an operating potential of around 0.8 V. As discussed below, the exact conditions for maximum efficiency depend on fuel composition, temperature, and pressure. The quantitative behavior of the maximum efficiency versus cell potential, as illustrated in Fig. 1, was explained and discussed by Sidwell and Coors using a somewhat different model [7] .

2. Thermodynamic efficiency model

With some reasonable assumptions, the efficiency (i.e., Eq. (2)) may be evaluated entirely thermodynamically. As a result, efficiency can be computed very easily over wide ranges of operating conditions. Model development is facilitated by thinking of fuel and air flow along channels separated by an MEA structure. As the fuel flows along the anode channel, it is continuously diluted with products of the electrochemical reactions (primarily CO_2 and H_2O). Consequently the local reversible potential E_{rev} decreases along the length of the channel. Electrochemical charge transfer, and hence power generation, requires that E_{rev} exceed the operating cell potential E_{cell}, which is assumed to be spatially uniform along the channel length. If the channel is sufficiently long, the local E_{rev} will eventually decrease to operating potential E_{cell}. At this point the current density vanishes and no more electric power can be produced. The effective length for power generation L_{eff} is the channel length at which $E_{rev} = E_{cell}$. It is at this point where the fuel utilization ε_U and fuel-cell efficiency ε are maximum. Although L_{eff} varies as a

function of MEA structure and operating conditions, it is interesting to note that both ε_U and ε are functions only of the inlet fuel composition—they are independent of MEA structure and fuel flow rate. However, if the channel length is less than L_{eff}, the actual fuel utilization ε_U and efficiency ε do depend on MEA structure and flow rates.

2.1. Reversible cell potential

The thermodynamic analysis begins with a global electrochemical-oxidation reaction as

$$\nu'_f\left(\sum_{k=1}^{K} n_{f,k}\chi_k\right) + \nu'_o\left(\sum_{k=1}^{K} n_{o,k}\chi_k\right) \leftrightarrows \sum_{k=1}^{K} \nu''_{f,k}\chi_k + \sum_{k=1}^{K} \nu''_{o,k}\chi_k. \quad (7)$$

The seemingly complicated nomenclature is needed to retain generality in the fuel and oxidizer mixtures [8]. The chemical symbol for the kth species (which may participate as a fuel, an oxidizer, or both) is written as χ_k. The mole fractions within the inlet fuel and oxidizer mixtures are given as $n_{f,k}$ and $n_{o,k}$. Stoichiometric coefficients for the fuel and oxidizer mixtures are given as ν'_f and ν'_o, and stoichiometric coefficients of the kth product species in the fuel and air channels are given as $\nu''_{f,k}$ and $\nu''_{o,k}$.

The stoichiometric coefficients are easily determined by balancing the reaction for particular fuel and oxidizer streams. Each species χ_k has a primary identity as a fuel, an oxidizer, a product, or an inert, and this identity plays an essential role in balancing the reaction to determine stoichiometric coefficients and in assigning charge transfer [8]. The reactant and product stoichiometric coefficients ν are determined to balance the reaction. Depending on the ion transport in the electrolyte, products may be formed in the fuel or the oxidizer channels. For example, in a polymer electrolyte membrane (PEM) cell the product H_2O is formed in the oxidizer channel, while for an SOFC the product H_2O is formed in the fuel channel. This difference is accommodated by specifying the use of either $\nu''_{f,k}$ or $\nu''_{o,k}$ to designate where the product is formed. The global reaction can be written in compact form as

$$\sum_{k=1}^{K} \nu'_k\chi_k \leftrightarrows \sum_{k=1}^{K} \nu''_k\chi_k, \quad (8)$$

where $\nu'_k = \nu'_f n_{f,k} + \nu'_o n_{o,k}$ and $\nu''_k = \nu''_{f,k} + \nu''_{o,k}$.

The number of electrons transferred by the global electrochemical reaction is determined from the half-cell reactions as

$$n_e = \sum_{k=1}^{K} \nu'_f n_{f,k} z_{f,k} = \sum_{k=1}^{K} \nu'_o n_{o,k} z_{o,k}, \quad (9)$$

where $z_{f,k}$ and $z_{o,k}$ are the charges associated with each fuel and oxidizer species.

Based on the chemical-potential balance, the reversible cell potential can be calculated from the Nernst equation as

$$E_{rev} = -\frac{\Delta G}{n_e F} = E^\circ + \frac{RT}{n_e F}\sum_{k=1}^{K}(\nu'_f n_{f,k} + \nu'_o n_{o,k} - \nu''_k)\ln\left(\frac{p_k}{p_0}\right), \quad (10)$$

where E° is the ideal Nernst potential at standard conditions ($p_0 = 1$ atm), p_k the partial pressure of the kth species, $R = 8.314\,\mathrm{J\,mol^{-1}\,K^{-1}}$ the universal gas constant, and F=96,485.309 C mol^{-1} is the Faraday constant. The ideal Nernst potential at the standard conditions is given as,

$$E^\circ = -\frac{\Delta G^\circ}{n_e F}, \quad (11)$$

where ΔG° is the change in standard-state Gibbs free energy between products and reactants of the global electrochemical reaction (Eq. (8)). Specifically,

$$\Delta G^\circ = -\sum_{k=1}^{K}(\nu'_f n_{f,k} + \nu'_o n_{o,k} - \nu''_k)\mu^\circ_k, \quad (12)$$

where μ°_k is the standard-state chemical potential of the kth species. The standard-state thermodynamic properties of ideal gases depend only on temperature T, and are readily available in databases such as in Chemkin [9]. Assuming H_2 is the only electrochemically active fuel species, the reversible cell potential can be written as,

$$E_{rev,H_2} = -\frac{\Delta G^\circ_{H_2}}{2F} - \frac{RT}{2F}\ln\frac{p_{H_2O,a}}{p_{H_2,a}\,p^{1/2}_{O_2,c}}, \quad (13)$$

with

$$\Delta G^\circ_{H_2} = \mu^\circ_{H_2O,a} - \mu^\circ_{H_2,a} - \frac{1}{2}\mu^\circ_{O_2,c}. \quad (14)$$

It is well known that CO is also electrochemically active. Assuming charge transfer via H_2 alone is justified by the fact that catalytic reaction of CO with H_2O to form H_2 and CO_2 is fast. Thus, the water–gas-shift process to produce H_2 competes favorably with the relatively slow CO electrochemical oxidation.

2.2. Reaction voltage

Assuming that the global reaction achieves equilibrium within the cell, it follows from species mass balances in fuel and oxidizer channels that

$$\dot m_{f,k,in} - \dot m_{f,k,out} = W_k(\nu'_f n_{f,k} - \nu''_{f,k})\frac{I_e}{n_e F}, \quad (15)$$

$$\dot m_{o,k,in} - \dot m_{o,k,out} = W_k(\nu'_o n_{o,k} - \nu''_{o,k})\frac{I_e}{n_e F}. \quad (16)$$

The net electric current produced within the cell is I_e. The species mass flow rates at the inlets and outlets of the fuel and oxidizer channels are represented as $\dot m_k$, and W_k are species molecular weights. Multiplying both of these equations by the species specific enthalpies (i.e., enthalpy per unit mass), which for a

uniform-temperature system are constants, and summing over all species yields

$$(\dot{m}h)_{\mathrm{f,in}} - (\dot{m}h)_{\mathrm{f,out}} = \frac{I_\mathrm{e}}{n_\mathrm{e}F}\sum_{k=1}^{K} W_k h_k(\nu'_{\mathrm{f}} n_{\mathrm{f},k} - \nu''_{\mathrm{f},k}), \tag{17}$$

$$(\dot{m}h)_{\mathrm{o,in}} - (\dot{m}h)_{\mathrm{o,out}} = \frac{I_\mathrm{e}}{n_\mathrm{e}F}\sum_{k=1}^{K} W_k h_k(\nu'_{\mathrm{o}} n_{\mathrm{o},k} - \nu''_{\mathrm{o},k}). \tag{18}$$

The total mass flow rates and enthalpies in each channel are represented as $\dot{m} = \sum \dot{m}_k$ and $h = \sum Y_k h_k$, where $Y_k = \dot{m}_k/\dot{m}$ are the species mass fractions. Adding these two equations and multiplying by the cell operating potential E_{cell} yields

$$E_{\mathrm{cell}}[(\dot{m}h)_{\mathrm{in}} - (\dot{m}h)_{\mathrm{out}}] = E^\circ_{\mathrm{h}} W_\mathrm{e}, \tag{19}$$

where $(\dot{m}h)_{\mathrm{in}} = (\dot{m}h)_{\mathrm{f,in}} + (\dot{m}h)_{\mathrm{o,in}}$ and $(\dot{m}h)_{\mathrm{out}} = (\dot{m}h)_{\mathrm{f,out}} + (\dot{m}h)_{\mathrm{o,out}}$. The net electric work (power) is written as $W_\mathrm{e} = I_\mathrm{e} E_{\mathrm{cell}}$ and a "reaction voltage" is defined as

$$\begin{aligned} E^\circ_{\mathrm{h}} &= \sum_{k=1}^{K} \frac{W_k h_k}{n_\mathrm{e}F}[(\nu'_{\mathrm{f}} n_{\mathrm{f},k} + \nu'_{\mathrm{o}} n_{\mathrm{o},k}) - (\nu''_{\mathrm{f},k} + \nu''_{\mathrm{o},k})] \\ &= \frac{1}{n_\mathrm{e}F}\sum_{k=1}^{K} W_k h_k[\nu'_k - \nu''_k] = -\frac{\Delta H}{n_\mathrm{e}F}. \end{aligned} \tag{20}$$

2.3. Thermodynamic efficiency

With the reversible potential written as $E_{\mathrm{rev}} = -\Delta G/n_\mathrm{e}F$ and using Eq. (19), the net cell efficiency can be written as

$$\begin{aligned} \varepsilon = \frac{W_\mathrm{e}}{\dot{m}_{\mathrm{f,in}}\,\Delta h_{\mathrm{f,in}}} &= \left\{\frac{E_{\mathrm{rev}}}{E^\circ_{\mathrm{h}}}\right\}\left\{\frac{E_{\mathrm{cell}}}{E_{\mathrm{rev}}}\right\}\left\{\frac{(\dot{m}h)_{\mathrm{in}} - (\dot{m}h)_{\mathrm{out}}}{\dot{m}_{\mathrm{f,in}}\,\Delta h_{\mathrm{f,in}}}\right\} \\ &= \varepsilon_\mathrm{R}\varepsilon_\mathrm{V}\varepsilon_\mathrm{U}. \end{aligned} \tag{21}$$

In other words, the cell efficiency is the product of a reversible efficiency ε_R, a voltage efficiency ε_V, and a utilization efficiency ε_U.

Eq. (21) is a closed-form expression for fuel-cell efficiency. However, as discussed below, using Eq. (21) requires evaluating $(\dot{m}h)_{\mathrm{out}}$, which requires assuming that the exhaust stream is in chemical equilibrium. It is important to note that Eq. (21) does not depend on cell structure or internal polarization losses. It does account for the fuel mixture, operating temperature and pressure, fuel utilization, and cell voltage. Achieving the thermodynamically predicted efficiency requires that the cell be as large as needed, with larger areas needed for cells with higher internal polarization losses.

2.4. Equivalent expressions for utilization

The definition for ε_U in Eq. (21) appears to be different from the one in Eq. (6). However, some further manipulation reveals that they are indeed the same. The potential heat release from complete oxidation of the inlet fuel stream can be represented in terms of the enthalpies of fuel, oxidizer, and final products as

$$(\dot{m}\,\Delta h)_{\mathrm{f,in}} = (\dot{m}h)_{\mathrm{f,in}} + (\dot{m}h)^{\mathrm{full}}_{\mathrm{o,in}} - (\dot{m}h)^{\mathrm{full}}_{\mathrm{p,in}}, \tag{22}$$

where $(\dot{m}h)^{\mathrm{full}}_{\mathrm{o,in}}$ is an "enthalpy rate" of the oxidizer required to fully oxidize the inlet fuel stream and $(\dot{m}h)^{\mathrm{full}}_{\mathrm{p,in}}$ is the enthalpy rate of the products of the completely oxidized initial fuel stream. An analogous relationship applies to the exhaust stream, which may contain unspent fuel,

$$(\dot{m}\,\Delta h)_{\mathrm{f,out}} = (\dot{m}h)_{\mathrm{f,out}} + (\dot{m}h)^{\mathrm{full}}_{\mathrm{o,out}} - (\dot{m}h)^{\mathrm{full}}_{\mathrm{p,out}}. \tag{23}$$

For a given fuel stream, the fully oxidized products must have the same enthalpy rates at the cell inlet and the cell outlet (i.e., $(\dot{m}h)^{\mathrm{full}}_{\mathrm{p,in}} = (\dot{m}h)^{\mathrm{full}}_{\mathrm{p,out}}$). Furthermore, the difference in the oxidizer required to completely oxidize the inlet and outlet streams must be provided from the cathode stream (i.e., $(\dot{m}h)^{\mathrm{full}}_{\mathrm{o,in}} - (\dot{m}h)^{\mathrm{full}}_{\mathrm{o,out}} = (\dot{m}h)_{\mathrm{o,in}} - (\dot{m}h)_{\mathrm{o,out}}$). It follows that

$$\begin{aligned} &(\dot{m}\,\Delta h)_{\mathrm{o,in}} - (\dot{m}\,\Delta h)_{\mathrm{f,out}} \\ &\quad = (\dot{m}h)_{\mathrm{o,in}} - (\dot{m}h)_{\mathrm{f,out}} + (\dot{m}h)_{\mathrm{o,in}} - (\dot{m}h)_{\mathrm{o,out}} \\ &\quad = (\dot{m}h)_{\mathrm{in}} - (\dot{m}h)_{\mathrm{out}}. \end{aligned} \tag{24}$$

Thus, the two representations of ε_U in Eqs. (6) and (21) are the same.

2.5. Algorithm for efficiency calculation

With two assumptions, the maximum fuel utilization can be determined. Assume first that the fuel cell is sufficiently large that all the fuel that can be consumed is consumed. In other words, the fuel content of the exhaust stream has been depleted and diluted to the point that $E_{\mathrm{rev}} = E_{\mathrm{cell}}$. Assume further that the exhaust mixture is in chemical equilibrium. For a given E_{cell}, the exhaust composition can be determined via the relationship between composition and E_{rev}. Because it is difficult to evaluate directly the numerator in Eq. (6), the following approach is followed.

The species molar flow rates at the inlet to the fuel and oxidizer channels are specified as $\dot{N}^{\mathrm{in}}_{\mathrm{f},k}$ and $\dot{N}^{\mathrm{in}}_{\mathrm{o},k}$. Assuming that some fraction γ of the inlet fuel is electrochemically oxidized via the global reaction (Eq. (7)), the outlet molar flow rates may be determined as

$$\dot{N}^{\mathrm{out}}_{\mathrm{f},k} = \frac{\dot{N}^{\mathrm{in}}_{\mathrm{f,\,tot}}}{\nu'_{\mathrm{f}}}[(1-\gamma)\nu'_{\mathrm{f}} n_{\mathrm{f},k} + \gamma\nu''_{\mathrm{f},k}], \tag{25}$$

$$\dot{N}^{\mathrm{out}}_{\mathrm{o},k} = \dot{N}^{\mathrm{in}}_{\mathrm{o},k} + \frac{\dot{N}^{\mathrm{in}}_{\mathrm{f,\,tot}}}{\nu'_{\mathrm{f}}}\gamma[\nu''_{\mathrm{o},k} - \nu'_{\mathrm{o}} n_{\mathrm{o},k}], \tag{26}$$

where $\dot{N}^{\mathrm{in}}_{\mathrm{f,tot}}$ is the total molar flow of the fuel stream at the inlet. In this way, both the fuel and air flow rates at the outlet can be defined in terms of a single parameter γ.

To calculate the reversible potential E_{rev}, both the outlet fuel stream and air stream are assumed to be in chemical equilibrium. The equilibrium species distributions are computed assuming the element balances associated with the molar flow rates at the channel outlets, $\dot{N}^{\mathrm{out}}_{\mathrm{f},k}$ and $\dot{N}^{\mathrm{out}}_{\mathrm{o},k}$. Thus, once the inlet flows and the

global reaction is specified, E_{rev} can be determined in terms of γ alone. By assuming that charge transfer proceeds entirely via H_2 oxidation, E_{rev} is determined from Eq. (13) with the partial pressures taken from the equilibrium compositions of the anode and cathode outlets.

Once the reversible potential E_{rev} equals the cell operating potential E_{cell}, no further fuel can be consumed electrochemically and no further power is generated. The maximum fuel consumption γ_{max} can be determined from the iterative solution of

$$E_{rev}(\gamma_{max}) = E_{cell}. \tag{27}$$

Once γ_{max} is determined, the corresponding compositions of the fuel and air streams at the outlets can be calculated. With the fuel composition at the outlet known, the heating value associated with full oxidation of the remaining fuel can be computed. Once $\dot{m}_{f,out}\,\Delta h_{f,out}$ is computed, ε_U is determined from Eq. (6). The net efficiency then follows from Eq. (21).

2.6. Effect of mass flow rate on efficiency

Assuming that the cathode-side air flow rate is sufficiently high that maximum fuel utilization can be achieved, the fuel-cell efficiency can be shown to be independent of the flow rate of the inlet fuel stream. The mass flow rate at the fuel-channel outlet can be represented as,

$$\dot{m}_{f,out} = \sum_{k=1}^{K} \dot{N}_{f,k}^{out} W_k, \tag{28}$$

Based on Eq. (25), the mass flow rate can be rewritten as,

$$\dot{m}_{f,out} = \dot{N}_{f,tot}^{in} \sum_{k=1}^{K} \frac{W_k}{\nu_f'}[(1-\gamma)\nu_f' n_{f,k} + \gamma\nu_{f,k}''], \tag{29}$$

or

$$\dot{m}_{f,out} = \frac{\dot{m}_{f,in}}{\bar{W}_{f,in}} \sum_{k=1}^{K} \frac{W_k}{\nu_f'}[(1-\gamma)\nu_f' n_{f,k} + \gamma\nu_{f,k}''], \tag{30}$$

where $\bar{W}_{f,in} = \sum_{k=1}^{K} n_{f,k} W_k$ is the mean molecular weight of the inlet fuel mixture. Therefore, the ratio of the mass flow rates at the outlet and the inlet of the fuel channel can be written as

$$\frac{\dot{m}_{f,out}}{\dot{m}_{f,in}} = (1-\gamma) + \gamma \frac{\sum_{k=1}^{K} (\nu_{f,k}''/\nu_f') W_k}{\sum_{k=1}^{K} n_{f,k} W_k}. \tag{31}$$

It is apparent the ratio of the mass flow rates, $\dot{m}_{f,out}/\dot{m}_{f,in}$, depends only on the composition of the inlet fuel mixture, the global electrochemical reaction, and the fuel utilization; it does not depend on the flow rate through the fuel channel. Thus, at γ_{max} where $E_{rev} = E_{cell}$, Eqs. (6), (21), and (31) indicate that both the fuel-cell efficiency and the fuel utilization are independent of the mass flow rates through the fuel and air channels.

2.7. Effects of cell voltage and fuel stream on efficiency

Fig. 2 shows maximum efficiencies and fuel utilization as functions of the operating cell voltage for several fuel streams.

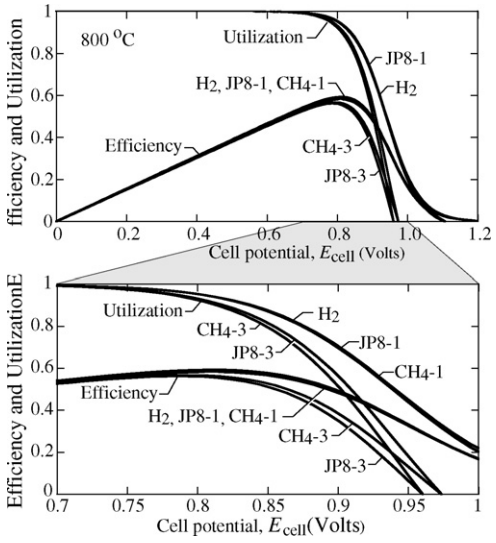

Fig. 2. The predicted maximum thermodynamic fuel-cell efficiency and fuel utilization as functions of cell voltage for different fuel streams at 800 °C and 1 atm. The fuel streams illustrated here include the pure H_2 fuel stream, the equilibrium composite fuel stream based on CH_4–steam and JP8–steam streams with the steam–carbon ratio of 1 (CH_4-1, JP8-1) and 3 (CH_4-3, JP8-3) at 800 °C and 1 atm. The lower panel is an expanded view for the operating voltages from 0.7 V to 1 V.

These include pure H_2 and mixtures of CH_4–steam, and JP8–steam. Steam–carbon ratios of 1 and 3 are considered, designated as CH_4-1, CH_4-3, JP8-1, and JP8-3. JP8 is assumed to be a mixture of 80.1% $C_{13}H_{28}$, 1.9% $C_{13}H_{26}$, and 18% $C_{13}H_{14}$. For the hydrocarbon–steam mixtures, the fuel that enters the fuel cell is the equilibrium composition at the fuel-cell temperature and pressure. Table 1 shows the equilibrium major-species mole fractions at 800 °C and atmospheric pressure for the four fuel–steam mixtures.

In all cases shown in Fig. 2, the cell is assumed to be isothermal at 800 °C, atmospheric pressure, and the cathode stream is undiluted air. The effects of the three contributing efficiencies are evident in the figure. At low cell voltage the efficiency increases linearly as a result of ε_V. In this region the utilization is nearly 100% and the slope of the efficiency function depends on the reversible efficiency ε_R. At around 0.8 V the utilization begins to fall, contributing to a decreasing efficiency. The utilization decreases because the operating voltage exceeds the reversible potential of the partially depleted fuel stream. At sufficiently high voltage, utilization (and hence efficiency) decreases to zero when none of the fuel can be electrochemically oxidized. The cell efficiency and

Table 1
Gas-phase equilibrium mole fractions for four fuel–steam mixtures at 800 °C and 1 atm

	CH_4-1	CH_4-3	JP8-1	JP8-3
CH_4	0.02674	0.00042	0.02764	0.00026
CO	0.22968	0.10792	0.31686	0.11644
H_2	0.71684	0.55761	0.62793	0.48120
H_2O	0.01979	0.27558	0.01775	0.31781
CO_2	0.00695	0.05846	0.00982	0.08430

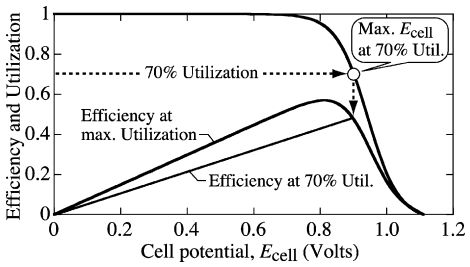

Fig. 3. Illustration of how the fuel-cell efficiency varies as a function of the operating cell potential for a given fuel utilization.

fuel utilization of CH_4–steam and JP8–steam fuel streams with the steam–carbon ratio of 1 are almost the same as those for the pure H_2 fuel stream. However, as more steam is added to the hydrocarbon fuels, the cell efficiency drops slightly, and the operating voltage for maximum efficiency also drops slightly.

There are often good reasons to operate the fuel cell itself at less than maximum efficiency, seeking to optimize overall efficiency of a full system. For example, excess fuel in the fuel-cell exhaust may be burned to provide heat needed in a recuperator to preheat the air stream prior to entering the fuel cell. Thus, the maximum efficiency and fuel utilization shown in Fig. 2 may not represent the best operating point. Rather, operating at reduced fuel utilization may be preferred. Fig. 3 illustrates the relationships of the maximum efficiency and utilization to efficiency at a specified utilization.

For fixed utilization (illustrated in Fig. 3 as 70%), the maximum-utilization function can be used to determine the maximum operating potential above which the fixed fuel utilization can no longer be achieved. At this maximum operating potential, the maximum-efficiency curve shows the maximum efficiency for the specified utilization. The straight line connecting the origin to this maximum efficiency represents the efficiency at fixed utilization.

At a given utilization, it is useful to know the maximum efficiency and operating potential needed to achieve the maximum efficiency. Fig. 4 shows maximum efficiency as a function of utilization for two methane–steam fuel mixtures. The figure also shows the operating potential needed to achieve the maximum efficiency. The information in Fig. 4 is identical to that in Fig. 2; it simply re-plots the data using utilization as the abscissa.

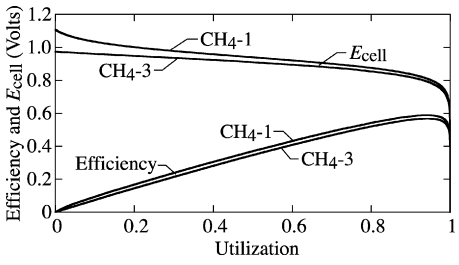

Fig. 4. Maximum fuel-cell efficiency and the corresponding operating potential as functions of maximum fuel utilization for CH_4–steam equilibrium fuel streams at a steam–carbon ratios of 1 (CH_4-1) and 3 (CH_4-3). In all cases the cell is at 1 atm and 800 °C.

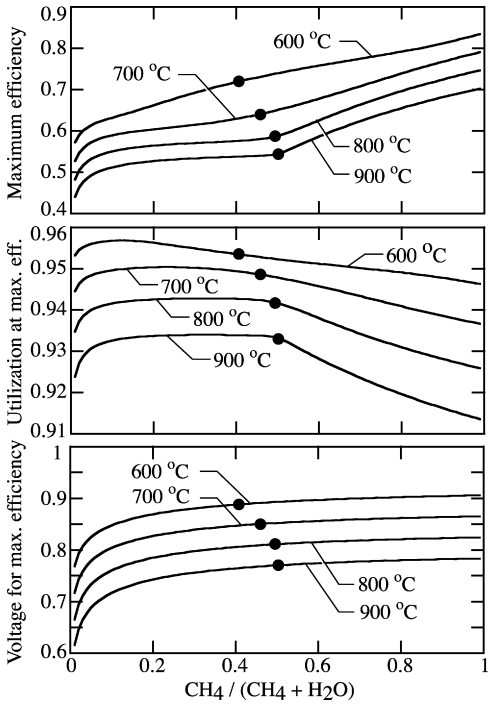

Fig. 5. Efficiency characteristics for SOFCs with methane–steam fuel mixtures. The abscissa is the mole fraction of methane in methane–steam mixture. The fuel that enters the fuel cell itself is the equilibrium composition that results from the given methane–steam mixture at the fuel-cell temperature and atmospheric pressure. The top panel shows maximum possible efficiency. The middle panel shows the utilization at maximum efficiency. The lower panel shows the operating potential needed to achieve maximum efficiency. The solid markers represent the points at which equilibrium predicts solid-carbon formation.

3. Efficiency maps

Because the thermodynamic models are so efficient computationally, it is easy to map large regions of parameter space. This can be helpful in identifying trends, seeking optimal operating conditions. Fig. 5 shows SOFC maximum-efficiency characteristics as functions of methane–steam mixtures and cell operating temperature. Clearly maximum efficiency increases as methane content increases. Reducing temperature also increases efficiency significantly. In all cases utilization is above 90% at maximum efficiency. The operating potential to achieve maximum efficiency increases substantially as operating temperature decreases. The solid markers on the curves represent the point at which chemical equilibrium predicts the formation of solid carbon. At methane concentrations above these levels, the systems design needs to consider coke formation that may degrade cell performance. If higher hydrocarbons also enter the fuel cell predicting deposit formation is more complex. In addition to surface-catalyzed coke formation, gas-phase routes can lead to polyaromatic hydrocarbon deposits [10,11].

4. Channel flow model and power density

It is interesting to compare the results of the thermodynamic-efficiency model with a much more detailed model that directly incorporates electrochemical charge-transfer kinetics, heterogeneous reforming kinetics, fuel and air flow in anode and cath-

ode channels, dense-electrolyte ion transport, and porous media transport in electrodes [4]. The detailed model confirms the predictions of the thermodynamic model. The detailed model also provides much more information, such as power density and thermal loads. The detailed model also provides a great deal of local information throughout the cell, none of which the thermodynamic model can deliver. Unlike the thermodynamic model, the detailed model requires very specific information about the cell architecture and the MEA, as well as operating conditions. For the sake of illustration the cell described by Zhu et al. [4] is used here in the detailed model. Summarized briefly, the anode is a 1.22-cm-thick porous Ni-YSZ cermet. The dense electrolyte is 8-YSZ that is 25 μm thick. The cathode is a 30 μm porous LSM structure. For the example here, the detailed model uses square channel cross-sections of 1 mm^2. The electrochemically active perimeter is 1.2 mm, which is 0.2 mm wider than the channel electrode interface. Other physical and chemical parameters, as well as details of the model, can be found in [4].

The upper panel in Fig. 6 illustrates the performance of the nominal MEA structure operating in a humidified H_2 fuel stream and a diluted H_2 fuel stream at 800 °C and 1 atm. To assist investigating the effects of the MEA performance on the fuel-cell efficiency, a reduced-performance MEA was constructed. Leaving all other cell parameters unchanged, the exchange current densities at the anode–electrode interface $i^*_{H_2}$ and at the cathode–electrolyte interface $i^*_{O_2}$ are both reduced to 1 A cm^{-2} (see Zhu et al. [4] for detailed definitions). The lower panel in Fig. 6 shows the MEA performance is significantly degraded.

Fig. 7 compares directly results from the thermodynamic and detailed models for a cell operating on a fuel stream mixture of 12% CH_4, 66% H_2, and 22% CO, which is essentially the gas-phase chemical equilibrium composition of an initial mixture of 60% CH_4 and 40% H_2O at 800 °C and 1 atm. The inlet velocity is 10 cm s^{-1}. The models predict virtually identical efficiency and utilization performance. This excellent comparison is observed over very large ranges of fuels and operating conditions. Furthermore, the efficiency and utilization predicted by the detailed model are virtually identical with either the nominal or reduced-performance MEA. However, as discussed below, when the reduced-performance MEA is used the cell must be much larger to achieve the maximum efficiency. Fig. 7 also compares the power density at the maximum fuel utilization for the two MEA structures. As expected, the power density for the performance-reduced MEA is much lower than that for the normal MEA. The different power densities lead to different channel lengths to achieve the same maximum efficiency. For the conditions in these examples, the nominal MEA results in a channel length of 9.1 cm to achieve the maximum efficiency of 63%. The reduced-performance MEA requires a much longer channel length of 17.9 cm.

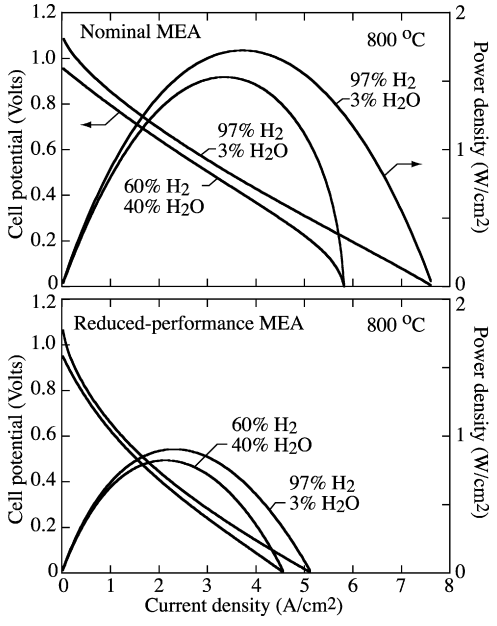

Fig. 6. Polarization characteristics for two MEA structures, each operating on H_2–H_2O fuel mixtures. The upper panel shows performance of the MEA that is described in Zhu et al. [4]. The lower panel shows a lower-performance MEA. In both cases the cells are operating at 800 °C and atmospheric pressure.

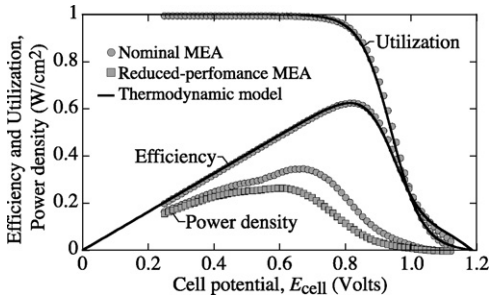

Fig. 7. Comparison of the maximum fuel-cell efficiency and fuel utilization calculated from the thermodynamic model and a detailed model [4]. The inlet fuel stream is the equilibrium composition resulting from an initial fuel mixture of 60% CH_4 and 40% H_2O at 800 °C and 1 atm. The fuel cell is operated at 800 °C and 1 atm. The overall power densities for the normal MEA and the performance-reduced MEA are calculated with the detailed model.

It is interesting to note that the power densities show maxima as functions of operating cell potential. The voltage for the peak power density is around 0.68 V for the nominal MEA in this example, and is reduced slightly to about 0.63 V for the performance-reduced MEA. In both cases the peak power density occurs at operating potentials well below the operating potential for maximum efficiency. From the fuel-cell design and optimization point of view, the fuel cell should be designed and operated to achieve appropriate tradeoffs between efficiency, utilization, and power density. The models described here provide tools that can be very effective in evaluating these tradeoffs.

5. Conclusions

Two models are developed and used to predict SOFC efficiencies for a wide range of fuels and operating conditions. The net efficiency is the product of a reversible efficiency, voltage efficiency, and fuel utilization. Cell efficiency is a strong function of operating voltage, with maximum efficiency achieved at cell voltages in the range of 0.8 V. The thermodynamic model predicts best possible performance, independent of specific cell design. The channel-based model incorporates details of MEA

structure, fluid transport, and charge-transfer, and reforming kinetics. Both models can be used to guide the optimization of cell design and operation.

Acknowledgments

This work was supported by the Office of Naval Research under a Multidisciplinary University Research Initiative (MURI) program (N00014-02-1-0665) and a Research Tools Consortium (N00014-05-1-0339). We gratefully acknowledge many insightful discussions about fuel-cell performance with Prof. David Goodwin (Caltech), Prof. Greg Jackson (University of Maryland), Prof. Tony Dean (Colorado School of Mines), Dr. Grover Coors, and Dr. Rod Sidwell (CoorsTek).

References

[1] Fuel Cell Handbook, seventh ed., Technical Report DOE/NETL 2004/1206, National Energy Technology Laboratory, Morgantown, WV, 2002, available at http://www.netl.doe.gov.

[2] A. Rao, J. Maclay, S. Samuelsen, Efficiency of electrochemical systems, J. Power Sources 134 (2004) 181–184.

[3] A. Lutz, R. Larson, J. Keller, Thermodynamic comparison of fuel cells to the Carnot cycle, Int. J. Hydrogen Energy 27 (2002) 1103–1111.

[4] H. Zhu, R. Kee, V. Janardhanan, O. Deutschmann, D. Goodwin, Modeling elementary heterogeneous chemistry and electrochemistry in solid-oxide fuel cells, J. Electrochem. Soc. 152 (2005) A2427–A2440.

[5] B. Thorstensen, A parametric study of fuel cell system efficiency under full and part load operation, J. Power Sources 92 (2001) 9–16.

[6] A. Ferguson, V. Ugursal, Fuel cell modelling for building cogeneration applications, J. Power Sources 137 (2004) 30–42.

[7] R. Sidwell, W. Coors, Large limits of electrical efficiency in hydrocarbon fueled SOFCs, J. Power Sources 143 (2005) 166–172.

[8] H. Zhu, R. Kee, A general mathematical model for analyzing the performance of fuel-cell membrane-electrode assemblies, J. Power Sources 117 (2003) 61–74.

[9] R. Kee, F. Rupley, J. Miller, The Chemkin Thermodynamic Data Base, Technical Report SAND87-8215, Sandia National Laboratories, 1987.

[10] G. Gupta, A. Dean, K. Ahn, R. Gorte, Comparison of conversion and deposit formation of ethanol and butane under SOFC conditions, J. Power Sources 156 (2006) 434–447.

[11] C. Sheng, A. Dean, The importance of gas-phase kinetics within the anode channel of a solid-oxide fuel cell, J. Phys. Chem. 108 (2004) 3772–3783.